Aerodynamic Flow Control using a Variable Droop Leading Edge Airfoil

M.S.Chandrasekhara
Navy-NASA Joint Institute of Aerospace Sciences
Department of Mechanical Engineering and Astronautics
Naval Postgraduate School, Monterey, CA 93943, USA

mchandra@nps.edu

C.Tung/P.B. Martin
Aeroflightdynamics Directorate, U.S. Army RDECOM
NASA Ames Research Center, M.S. 215-1, Moffett Field, CA 94035, USA

ctung@mail.arc.nasa.gov/pmartin@merlin.arc.nasa.gov

ABSTRACT

Control of dynamic stall under compressible flow conditions appropriate for a helicopter rotor has been demonstrated using a variable droop leading edge airfoil. The airfoil leading edge is drooped in phase with its sinusoidal pitch oscillations to eliminate the dynamic stall vortex that induces many adverse effects on the blade. The approach results in dramatic reductions in drag and pitching moment, while also decreasing the maximum lift slightly. This loss was recovered using a trailing edge mounted vertical Gurney flap of 1% chord height, without undue drag penalty. Drooping the leading edge substantially modifies the airfoil pressure distributions such that the dynamic stall onset mechanism is changed from shock-induced to pressure gradient induced for certain flow conditions. The changes also manifest in significantly lowered peak vorticity fluxes preventing the flow vorticity from coalescing into a very tightly organized dynamic stall vortex. The behavior of transition and its role in the process are also addressed.

1.0 INTRODUCTION

It is widely recognized that flow separation has placed the most significant limitation on the performance of all flight vehicles for both steady and unsteady conditions. Dynamic stall is a particular class of unsteady flow separation that occurs when an airfoil is pitched rapidly past the static stall angle. Compressibility effects set in at low to moderate flight speeds (Mach number = 0.2 to 0.3) in this class of flows. Onset of compressibility promotes premature separation (i.e., stall occurs at lower angles of attack) with the separation process manifesting dramatically differently [1]. One example is: trailing edge stall seen at low speeds becomes an abrupt leading edge stall. The details of stall the onset process differ depending upon parameters of the imposed unsteady motion and flow conditions. For this paper, a large amplitude sinusoidal motion that typifies a rotor blade cyclic pitch motion will be considered since compressible dynamic stall is an acute problem for a helicopter. Such a motion naturally results in angles of attack that exceed the static stall angle by a wide margin. The performance of a rotorcraft becomes severely limited if dynamic stall ensues under such unsteady motion. The process also introduces new and complicated physics to the flow vorticity field. Primarily, the vorticity production and diffusion need to be in balance during each oscillation cycle without

Paper presented at the RTO AVT Specialists' Meeting on "Enhancement of NATO Military Flight Vehicle Performance by Management of Interacting Boundary Layer Transition and Separation", held in Prague, Czech Republic, 4-7 October 2004, and published in RTO-MP-AVT-111.

notable hysteresis for ensuring stable performance. However, when the production exceeds diffusion through the boundary layer, dynamic stall onset occurs as an abrupt coalescence of the large amount of vorticity in the flow and the vorticity being shed as the dynamic stall vortex. Its passage over the airfoil introduces a dramatic movement of the center of pressure leading to violent pitching moment fluctuations. The unfavorable consequences of these on the vehicle make it imperative to prevent the formation of the dynamic stall vortex altogether. Thus, even though the dynamic stall vortex can add to the total rotor lift by producing large dynamic lift from the naturally present unsteady motion of the blade the setting machine controls restrict flying in this portion of the envelope.

Once compressibility effects set in, the dynamic stall onset mechanism changes for even slight increases in freestream Mach number. For example, as shown in Fig. 1a for a freestream Mach number, M = 0.3 and reduced frequency, k = 0.1, dynamic stall occurs purely from a large adverse pressure gradient due to the extremely high value of suction developed near the airfoil leading edge. Earlier studies [2] have shown that the formation of the dynamic stall vortex is an abrupt event. The value of the adverse pressure gradient at which it forms depends on the state of the local boundary layer whether there is transition occurring and whether there is a laminar separation bubble present. Chandrasekhara et al [1] show that the value can be very low under certain conditions in the presence of a bubble. Once the vortex forms, it convects over the airfoil upper surface. The imprint of this convection appears as a mobile pressure peak with increasing angle of attack. For M = 0.3, at all non-zero reduced frequencies tested it was found that the peak value of suction, while being high was only slightly higher than C_p^* (= -7.0) and so could only induce a weak supersonic flow but not strong shocks.

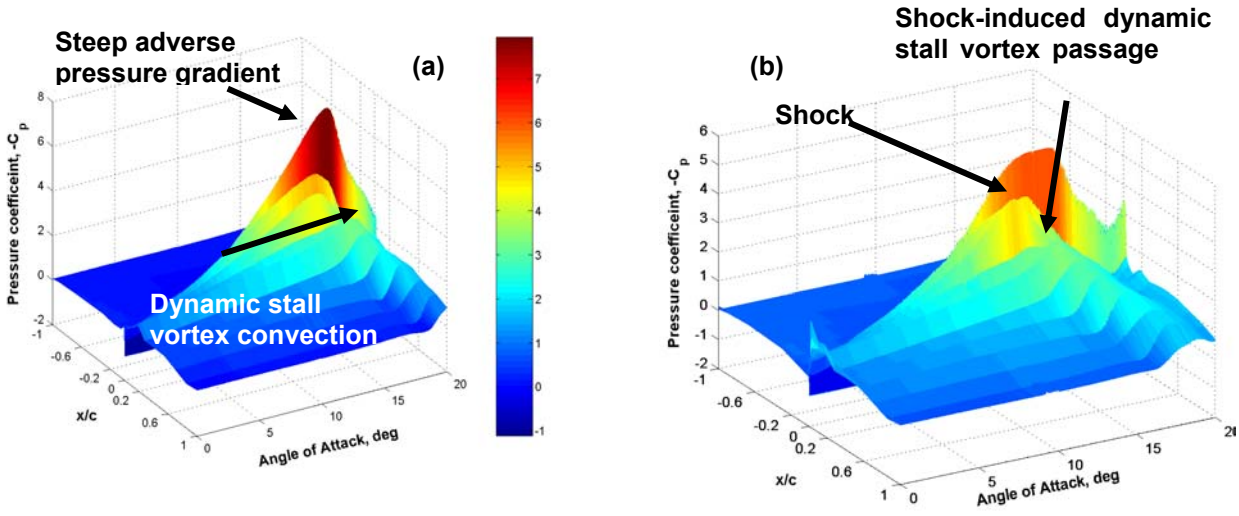

Fig. 1. Airfoil surface pressures over a complete oscillation cycle of a VR-12 airfoil showing different dynamic stall onset processes, k = 0.1, $\alpha = 10^O\text{-}10^O \sin\omega t$ (a) M = 0.3 (b) M = 0.4 [3]

At a freestream Mach number of 0.4, Fig. 1b shows that shock induced dynamic stall occurs since the local flow is strongly supersonic, ($C_{p_{min}} \approx$ -4.5, C_p^* = -3.66). Interferograms of this flow actually show that multiple shocks form, the last one in the series is a strong normal shock, the pressure rise across which is large enough

to cause separation. The consequence of such separation is an elongated vortex [1] which as it convects over the airfoil leaves a pressure imprint similar to that seen for M = 0.3. In all situations (steady or unsteady), the boundary layer vorticity is either shed immediately in a sheet as in steady stall – or, becomes wound into a tight vortex - dynamic stall. The phenomenon is also governed by the state of the boundary layer and its ability to withstand the forces causing separation. At model rotor Reynolds numbers, transition point movement, due to the large angle of attack changes involved, becomes an additional, dominant flow factor. Further complexity is introduced when surface unsteadiness is involved through the interaction of the time scales of the flow. A mismatch of these scales actually leads to the coalescence of the vorticity into the vortex. Thus, dynamic stall control requires preventing the vortex from forming and managing the vorticity to gradually diffuse it at a rate consistent with its production in order to sustain the lift to high angles of attack. This is a formidable task. Despite the development of many approaches over the years, success is confined to a narrow range of flow conditions, beyond which the techniques consume sizeable system resources that make them unattractive. The present study recognized that flow control in this environment requires active *vorticity management* and attempted it. In this particular application, it is absolutely critical to prevent the formation of the dynamic stall vortex to avoid the pitching moment fluctuations that are detrimental to the structure of the vehicle. Hence, the degree of success of any dynamic stall control approach should be defined by this metric. Since vorticity is an intractable quantity and cannot be directly measured, indirect methods of quantifying the vorticity field become necessary. In this context, the following equation [3] offers some insight into the flow dynamics by establishing that the normal vorticity flux (LHS) is related to the surface acceleration (term I,

$$\nu \frac{\partial \Omega}{\partial n} = \frac{\partial U_S}{\partial t} + \frac{1}{\rho}\frac{\partial p}{\partial s} + V\Omega \qquad (1)$$

RHS), potential flow pressure gradient (term II) and surface transpiration (term III) respectively. The traditional suction/blowing approaches exploit the influence of term III to produce the observed benefits, with well-known limitations under compressible conditions. In this study, we introduced a controlled geometry change by variably drooping the leading edge of an airfoil, over a range of unsteady flow conditions of interest to a rotorcraft and maneuvering fighter aircraft. It will be demonstrated that the extremely large peak vorticity fluxes that naturally occur prior to stall onset are greatly diminished and so, the flow remains attached until higher angles of attack than observed hitherto in compressible dynamic stall.

2.0 DESCRIPTION OF THE EXPERIMENT

2.1 The Compressible Dynamic Stall Facility

The experiments were conducted in the Compressible Dynamic Stall Facility (CDSF) at NASA Ames Research Center. The CDSF is a continuous running in-draft wind tunnel with a 25 cm x 35 cm test section, powered by a 110 m^3/s, 9000 HP compressor. It is equipped with a drive for producing a sinusoidal variation of airfoil angle of attack. A choked downstream throat controls the flow in the tunnel. The flow conditions can be varied as follows: 0 ≤ freestream Mach number, M ≤ 0.5, 0 ≤ reduced frequency, $k = \pi fc/U_\infty \leq 0.1$ (f = oscillation frequency, c = airfoil chord and U_∞ = freestream velocity), $\alpha = \alpha_m + \alpha_a \sin\omega t$, where, 0 ≤ mean angle of attack, $\alpha_m \leq 15$ deg, and 2 ≤ amplitude of oscillation, $\alpha_a \leq 10$ deg. Inside the test section, the airfoil is held between two 2.54 cm thick oscillating metal sections (windows) using tangs. Optical quality glass inserts in these metal sections provide optical access allowing light to pass through the test section around the airfoil leading edge making direct visualization of the front 40% of the airfoil chord possible. The VDLE drive linkage connects externally on either side of the test section to anchor points outside. Presently, two modes of operation are possible. In the first one, the leading edge droop is set at a fixed value in the range 0 to –25 deg,

locked and the fixed-droop airfoil is oscillated over a range of flow conditions (Mach numbers from 0 to 0.45, reduced frequencies from 0 to 0.1 for angles of attack up to 25 deg). In the second mode, the airfoil droop is initially set at a value equal to or greater than the amplitude of oscillation and the airfoil is oscillated at the above conditions. In this mode, the droop variation is always phase locked to the oscillating airfoil angle of attack. These two modes of operation are respectively controlled by whether the external linkage is anchored to the oscillating window or to the stationary sidewall.

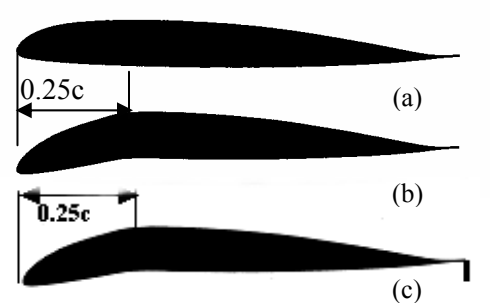

Fig. 2. (a) The original VR-12 compared with (b) the VR-12 VDLE profile (c) VDLE with Gurney flap

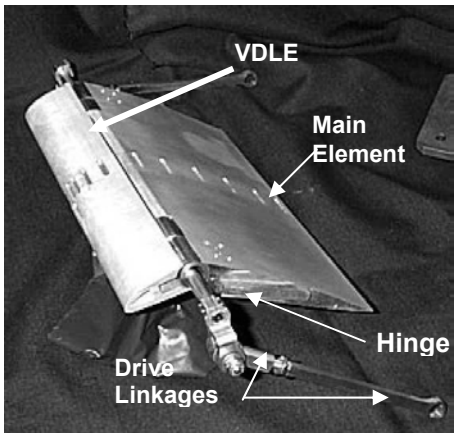

Fig. 3. Assembled VDLE airfoil

2.2 The Variable Droop Leading Edge (VDLE) Airfoil

Figure 2 shows the VDLE airfoil tested with Fig. 3 providing some details of the model assembly [4]. The base airfoil section was VR-12, Fig. 2a, with 15.24 cm chord and 25.4 cm span. The leading 25% of the airfoil was attached to a hinge at the quarter-chord point to produce various droop angles, Fig. 3. Fig. 2b shows the drooped leading edge mode of operation and Fig. 2c, a schematic of the airfoil with a Gurney flap attached to its trailing edge, [5]. Three different flaps were tested, but only results for the 1% chord nominal height flap are included in this paper. The hinge was attached to the main element held by rectangular tangs machined in the CDSF oscillating metal sections. The main element oscillated synchronously with the windows. The matching hinge on the drooping front portion of the airfoil was hollow (for carrying instrumentation leads and protruded from CDSF windows) and was connected to drive linkages (see Fig. 3) on either side of the test section. If these linkages were anchored to the oscillating windows, a fixed droop resulted through the oscillation cycle, if anchored to the fixed tunnel sidewalls, a variable droop leading edge (VDLE) mode of operation resulted, with the droop varying as: droop = α + initial droop angle.

2.3 Instrumentation and Techniques

The model was instrumented with 20 flush-mounted Kulite unsteady, absolute pressure, sealed gage, transducers at locations listed in Table 1, with 10 transducers on the drooping front portion and the rest on the main element on both upper and lower surfaces. The power supply and signal leads from these transducers were drawn through the hollow hinge shaft at the quarter chord point. The transducers were powered by a 15 V DC power supply. The signal from each channel was conditioned individually and those from all channels

were digitized simultaneously with a high speed (Microstar Laboratories) analog to digital converter and recorded with a data acquisition system that read the analog signals concurrently with the digital encoder signal of the airfoil instantaneous angle of attack using custom developed LabVIEW software. Typical sampling rates used were 4 KHz/channel with 40 000 samples/channel. At the oscillation frequencies used (up to 30 Hz), a sufficiently large number of realizations occurred with this approach. The data was ensemble averaged after randomly initiating the acquisition and later sorting it into 800 bins, each one-encoder count wide (corresponding to angle of attack bins of 0.002 to 0.08 deg depending on the phase angle through the sine wave of oscillation cycle for $\alpha = 10^{o} - 10^{o}\sin\omega t$). Anywhere from 40 to100 samples were present in each bin. The standard deviation of the data was generally low (less than 3% when flow was attached) yielding a low uncertainty for the measured ensemble averaged unsteady pressures. The transducers also had excellent temperature stability specifications [4].

The transducers were calibrated individually by enclosing them in a suction cup that was evacuated using an ISO 9000 certified Mensor pressure calibration unit over the anticipated range of pressures. The CDSF is an in-draft wind tunnel drawing air from the atmosphere and discharging into an evacuation compressor. Thus, the maximum pressure anywhere in the flow was atmospheric, with only suction at all locations over the airfoil. All 20 transducers were found to be linear over the range tested. Since absolute pressures were measured, considerable care was taken during calibration and experimentation to account for changes in ambient pressure (caused by weather front movements), noise, drift and such extraneous factors. The wind tunnel stagnation pressure, the static pressure and the dynamic pressure were measured using a Setra differential pressure transducer, with a verification of the ambient pressure from the Mensor calibration unit. Thus, it was possible to account for any drifts or environmental effects.

Table 1: Locations of the Pressure Taps on the VDLE Airfoil

Upper Surface	x/c	Lower Surface	X/c
1	0.000	1	0.010
2	0.010	2	0.025
3	0.025	3	0.050
4	0.050	4	0.150
5	0.100	5	0.300
6	0.175	6	0.500
7	0.275	7	0.700
8	0.400	8	0.900
9	0.550		
10	0.700		
11	0.850		
12	0.95		

Quantitative flow visualization was conducted using the real time technique of Point Diffraction Interferometry (PDI). Details of the PDI technique are provided in [6]. Several interferograms were acquired for each flow condition. Although PDI is a quantitative technique, the interferograms are used here only for their qualitative value because, the field of view was limited to x/c = 0.4 and the pressure data was available over the whole airfoil.

2.4 Calculation of C_l, C_d, C_m and Vorticity Flux

As stated earlier, the measured instantaneous voltages were sorted into 800 bins prior to saving the data. The contents of these bins were converted to pressures using the calibrations for the respective transducers; the mean and standard deviation of each bin data set was computed for the pressure coefficient. The lift, drag and pitching moment coefficients were calculated for each bin from the normal and axial forces computed by integrating the pressure coefficients, knowing the sensor spacing and the airfoil geometry. The viscous contribution to the drag was not recorded by wake surveys. Hence, these drag results represent only the form drag. Due to the absence of transducers at the trailing edge, the pressure there was set to be the average of the measured pressures closest to it by the upper and lower surface sensors to complete the integration process in all cases, [4].

For the fixed droop cases, the transducer locations were transformed along the main element chord line, as is standard practice in high lift device aerodynamics. For the VDLE cases, the transformation was carried out for each instantaneous angle of attack.

Since the Gurney flap was not instrumented, the pressures on its upstream and downstream faces were not measured. Thus, it was not possible to calculate the drag due to the flaps.

The surface vorticity fluxes were derived from the measured pressure distributions using a cubic spline curve fit to the data and interpolating the fitted pressures at 162 points on the airfoil upper surface. These points corresponded to the airfoil coordinates that were generated when the airfoil surface was measured in the metrology shop to ascertain its shape accurately. The pressure gradient was calculated from the curve fit and used as the surface vorticity flux by ignoring the surface acceleration term since an order of magnitude analysis showed it to be substantially smaller.

2.5 Experimental Conditions

The experimental data was obtained for:

Mach number, M:	0.2, 0.3, 0.4
Reduced frequency, $k = \pi fc/U_\infty$:	≈ 0 (quasi steady), 0.05, 0.1
Droop angle, δ:	0, 10, 20 deg; for the VDLE case, $\delta(t) = \alpha(t)$
Angle of attack, $\alpha(t)$:	$10^O - 10^O \sin\omega t$
Reynolds Number, Re:	$0.7 \times 10^6 - 1.6 \times 10^6$

The (quasi) steady flow data actually corresponds to a slow oscillation of the airfoil at $k \approx 0.002$.

2.6 Experimental Uncertainties

The following uncertainties have been estimated for the various quantities:

Mach number	± 0.005
Angle of attack:	0.05 deg
Reduced frequency:	0.005
C_p	±0.05 at M = 0.3
Vorticity flux	± 25 near the leading edge
C_l, C_d and C_m:	0.05, 0.05, and 0.005

3.0 RESULTS AND DISCUSSION

3.1. Point Diffraction Interferograms of Flow at M = 0.4, k = 0.1

Figure 4 presents typical flow visualization images recorded for M = 0.4, k = 0.1 and $\alpha = 10^{O}\text{-}10^{O}\sin\omega t$ for the VR-12 airfoil (top row images) and for the case of fixed droop angle of 10 deg (bottom row). These pictures show the instantaneous, spanwise averaged density contours in the flow and as such are representative of the pressure distributions as well when the flow is attached. A higher number of fringes locally represents a higher suction value in the accelerating flow regions around the leading edge. Fig. 4a for α = 14 deg shows that a series of shocks forms in the flow (due to local transonic flow over the laminar boundary layer) which culminate in a normal shock. The Mach number at the foot of the normal shock is in excess of 1.4, giving a pressure rise across it that is sufficient to induce flow separation. Images at slightly higher angles of attack (not shown) confirm that a dynamic stall vortex forms soon after and convects over the upper surface. The flow quickly reaches the deep dynamic stall state (Fig. 4b, α= 20 deg). In contrast, when a fixed droop of 10 deg is introduced to the leading edge element and the airfoil oscillated at the same conditions, Fig. 4c shows that the flow is fully attached at α = 14 deg. A large difference in the number of fringes between Fig. 4a and Fig. 4c for the same flow conditions confirms that the local flow acceleration is dramatically reduced when the airfoil is drooped. In this case, the flow remains subsonic at α = 14 deg because of this geometry change. Fig. 4b and Fig. 4d show that while the flow over the basic VR-12 airfoil is completely separated, that over the drooped airfoil remains attached over its leading section and only a mild trailing edge separation is seen over its rear section. Most noteworthy here is the absence of the dynamic stall vortex for the drooped case in the pictures and hence, its negative consequences. It is possible that a dynamic stall vortex formed downstream on the airfoil surface not visible in these images, which implies that it will be a weak one because of the reduced local adverse pressure gradients. The fact that there are still a number of fringes over the leading edge region affirms that the airfoil continues to develop a strong suction and hence, suction lift. These images demonstrate that flow control is achieved by drooping the airfoil. However, a fixed droop is not desirable over the full rotor blade cycle (and for fixed wings). Thus, a variable droop leading edge was pursued for further studies.

3.2. Airfoil Performance

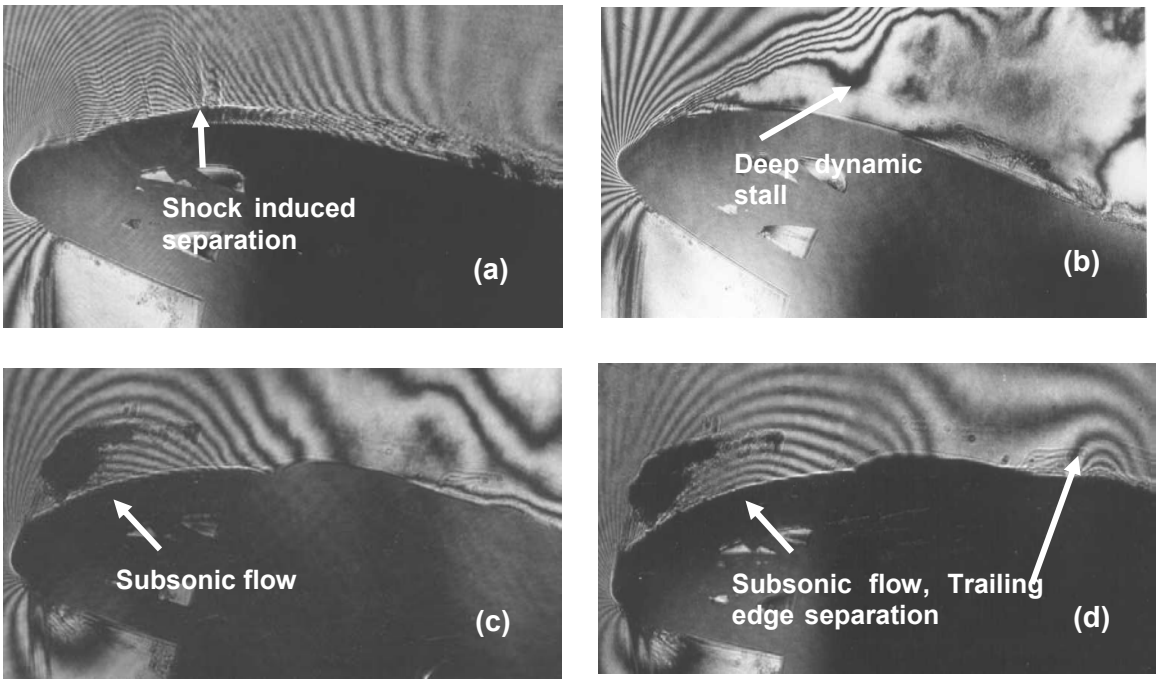

Fig. 4. PDI images of oscillating airfoil flow at M = 0.4, k = 0.1, $\alpha = 10^{O}$-10^{O} sinωt Top row: VR-12 airfoil, Bottom row: Fixed droop δ = 10 deg; Left Column: (a, c) α = 14 deg, Right Column: (b, d) α = 20 deg [4]

Of critical importance to any flight vehicle is the performance of the system. Fig. 5a presents the lift coefficient variation over the whole oscillation cycle for M = 0.3 with similar results shown in Fig. 5b for M = 0.4. The basic VR-12 airfoil shows the classical dynamic stall behavior with the lift increasing steadily as the airfoil is pitched up. Around α = 16 deg, there is slight drop which is followed by a rapid increase of C_{lmax} to $\approx$ 2.0, at a rate greater than the normal lift curve slope, a change attributable to the dynamic stall vortex. However, deep dynamic stall quickly ensues as the vortex convects past the airfoil trailing edge. This is evidenced by the steep drop in C_l near the top of the upstroke. The flow appears to reattach fully only towards the end of the downstroke where the lift values match those on the upstroke (at $\alpha \approx$ 2-3 deg), the large hysteresis loop is a manifestation of this situation. Thus, the flow over much of the downstroke remains separated for this flow condition. Results for the VDLE airfoil show that its lift curve slope is slightly smaller than that for the basic airfoil, but the airfoil continues to generate lift until α = 18 deg and the large amount of vorticity commensurate with such lift production is shed gradually. The gradual drop in lift indicates that the shedding of the vorticity is a more gradual process for the VDLE airfoil. It is worth noting here that since the PDI images for the fixed droop airfoil did not show a vortex on the upstroke, a similar result could be expected for the VDLE airfoil. But, the VDLE airfoil produces about 10-15% less peak lift than the base line airfoil. Load capabilities demanded from future helicopters require maximizing all aspects of their performance. Hence, it is important to recover some of this "lost" lift, which was attempted by adding a passive device in the form of a Gurney flap. Many different flap geometries are possible, here only a vertically mounted Gurney flap of different heights, attached to the trailing edge was tested. A satisfactory flap height

for the purpose of recovering the lift without undue drag penalty was determined to be approximately 0.01c. Fig. 5a includes the lift result for this case and it is seen that even such a small passive device shifts the lift curve to substantially higher values. In the VDLE mode of operation, this Gurney flapped airfoil indicated a lift behavior that far exceeded the values obtained by original VR-12 and the VDLE airfoils. The C_{l_0} value is about 0.5 and $C_{l_{max}} \approx 2.1$. Pressure distributions presented later show that this increase in lift can be attributed to the higher average positive pressure on the airfoil lower surface.

An almost identical behavior is observed in Fig. 5b for M = 0.4 also. Thus, a notable improvement in lift performance was achieved by the use of the VDLE concept, with further improvements through the addition of a 1% Gurney flap.

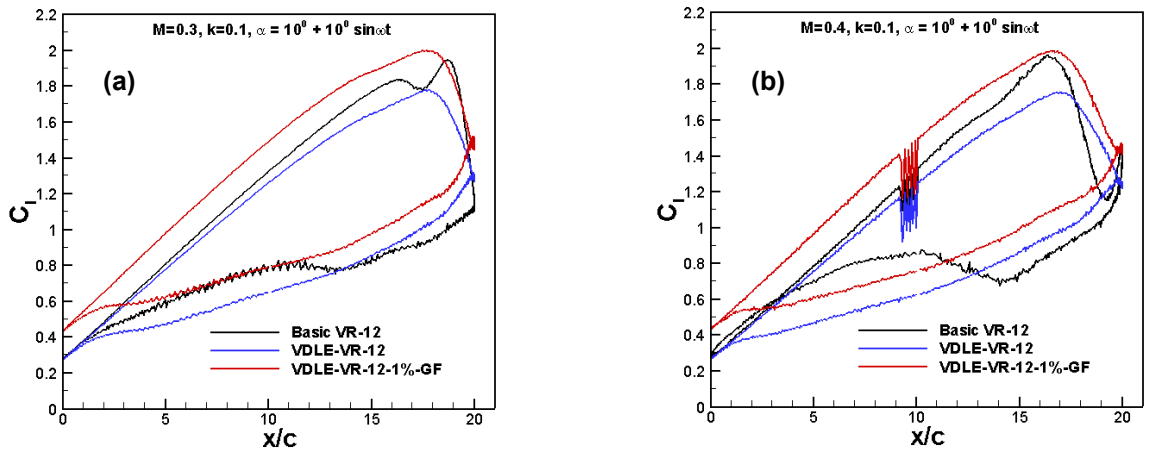

Fig. 5. Comparison of lift coefficient over a complete oscillation cycle
k = 0.1, $\alpha = 10^{O}$-10^{O} sinωt; (a) M = 0.3, (b) M=0.4

Figure 6 compares the drag behavior for the cases discussed above, with Fig. 6a for M = 0.3 and Fig. 6b for M = 0.4. The large drag rise seen for the VR-12 airfoil at both M = 0.3 and M =0.4 is clearly due to the formation of the dynamic stall vortex, which when shed causes a wake with a large defect. The vortex forms around α = 15-16 deg for M = 0.3 and around 12 deg soon after the shock forms for M = 0.4. For the VDLE airfoil case, the peak drag at both Mach numbers is about 50% – 75% lower and this is because no dynamic stall vortex formed in these cases. With the Gurney flap present, the drag is only slightly higher, yet considerably smaller than that for the VR-12 airfoil. (Non-inclusion of the viscous drag and fewer pressure taps in the trailing edge region are suspected to be the cause of a few negative counts of drag seen at lower angles in the figures). Despite the fact that the flap was not instrumented, a higher drag is measured for this case. The effects of the flap are felt on the overall pressure distributions by communication from the wake through the outer elliptic flow field. The addition of the flap has introduced only a slight drag penalty, but enabled recovering the full lift capability of the airfoil and thus, seems like a viable flow control option in combination with the VDLE concept.

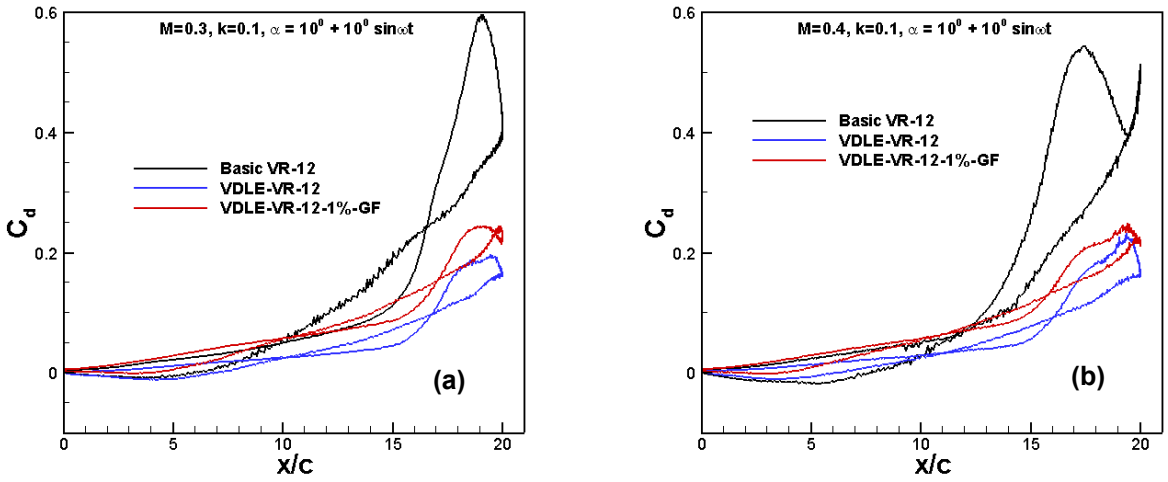

Fig. 6. Comparison of drag coefficient over a complete oscillation cycle
k = 0.1, $\alpha = 10^{O}$-10^{O} sinωt; (a) M = 0.3, (b) M=0.4

The limiting performance element for a helicopter is the pitching moment distribution. The violent fluctuations that accompany the dynamic stall vortex convection over the surface can severely reduce the fatigue life of a rotor blade and thus, need to be eliminated. It may be recalled here that successful flow control was defined earlier as, at least, mitigating the large negative pitching moment during the oscillation cycle. Fig. 7 shows that dynamic stall occurrence on the VR-12 airfoil results in a large negative pitching moment, with the value increasing from -0.1 to about -0.45 in about 3-4 degree angle of attack change once the vortex forms. The pitching moment loop also has crossovers that can lead to negative damping and cause additional structural problems. The VDLE airfoils without and with the flap both show a greatly reduced negative pitching moment peak, with the value increasing gradually with airfoil angle of attack. Since, the loop does not show large negative values and any crossovers, it is believed that no or only a weak dynamic stall may have formed in this case. The area under the loop is positive and leads to positive damping, a fact that is of immense value to designers and the structural integrity of the rotor blade. The offset seen for the Gurney flap case is due to the generally higher average pressure on the lower surface towards the trailing edge, that tends to produce a slightly nose down moment. Results shown in Fig. 8b for M = 0.4 are once again similar to those at M = 0.3 confirming the applicability of the VDLE concept to this higher Mach number situation, where the dynamic stall onset mechanism is notably different form the lower M = 0.3 case. Thus, it can be concluded that the VDLE airfoil concept is a viable flow control concept.

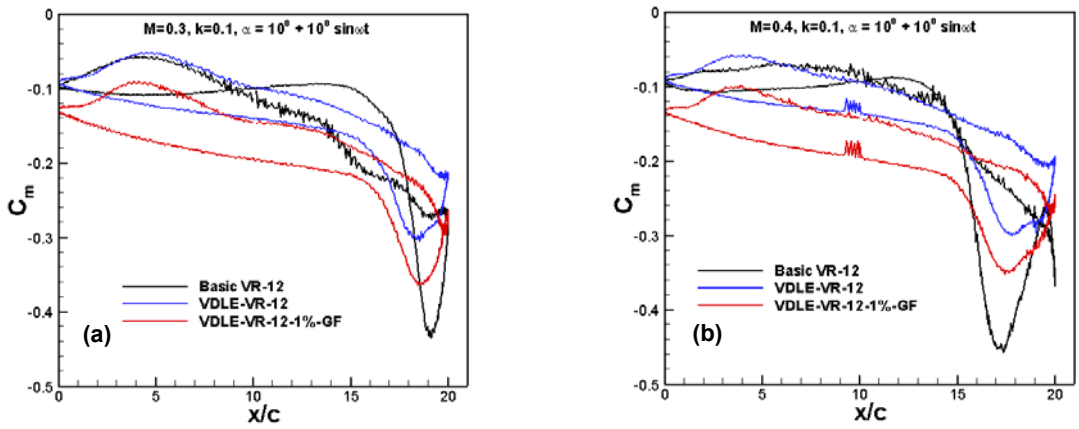

Fig. 7. Comparison of pitching moment coefficient over a complete oscillation cycle k = 0.1, $\alpha = 10^{O}\text{-}10^{O}\sin\omega t$; (a) M = 0.3, (b) M=0.4

3.3 Airfoil Pressure Distributions

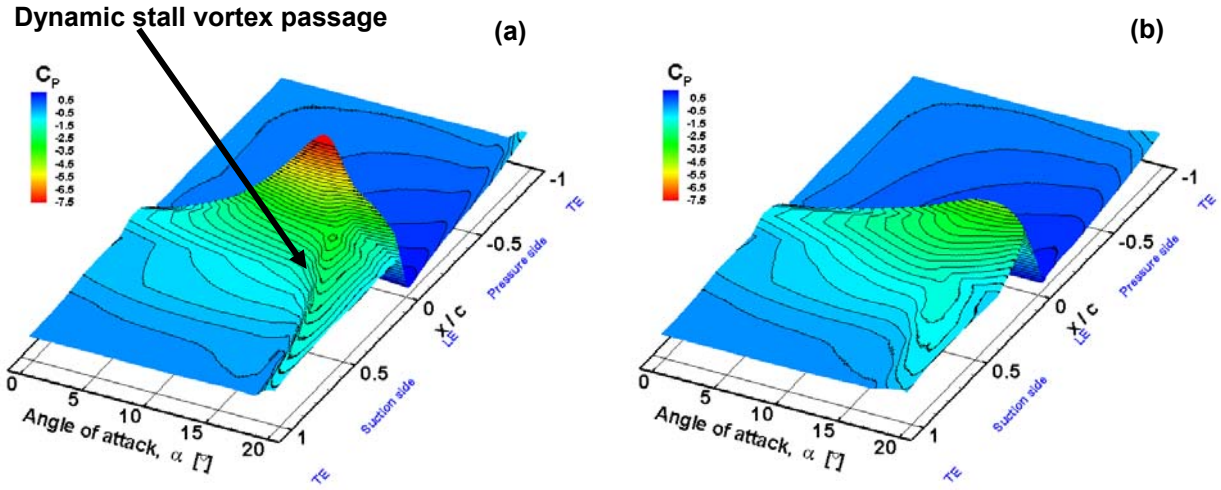

Fig. 8. Comparison of airfoil surface pressures over a complete oscillation cycle M = 0.3, k = 0.1, $\alpha = 10^{O}\text{-}10^{O}\sin\omega t$; (a) VR-12 airfoil (b) VDLE airfoil [6]

In an effort to establish the reasons for the dramatic improvement in performance observed with the use of the VDLE concept, the ensemble averaged pressures over the airfoil upper and lower surfaces are compared in Figs. 8a and 8b for the VR-12 and the VDLE airfoils respectively. The large suction developed by the VR-12 airfoil is clear in Fig. 8a. The value nearly reaches the critical pressure coefficient and the resulting steep adverse pressure gradient produces the dynamic stall vortex close to the leading edge, which convects as shown. The rapid drop in suction near the leading edge and at other locations as the vortex passes can be distinctly seen. This picture of the pressure distribution is similar for all pressure-gradient induced dynamic stall flow cases. Fig. 8b contrasts this picture with that for the VDLE airfoil when the dynamic stall process is

effectively controlled. By drooping the airfoil at a rate such that droop = angle of attack, the airfoil leading edge is always maintained at an incidence of zero degrees and thus, this portion of the airfoil can not produce the very large suction peaks appropriate for the instantaneous angles of attack of the airfoil. As shown earlier in Fig. 5, this results in some loss of lift relative to the VR-12 airfoil, however, the airfoil also does not experience stall on the upstroke from the leading edge. Representative PDI images for the fixed droop case indicated some trailing edge stall occurred even at α = 20 deg with no leading edge stall, so for the VDLE airfoil also a similar result seen can be expected. Consequently, if a dynamic stall vortex formed here at all, it would be a weak one. Fig. 4b suggests that it may have originated beyond x/c = 0.25 and the mild pressure imprint suggests that it is a weak one. It is also possible that it may not be shed on the upstroke also. Since the vorticity associated with the production of this lift has to be shed during each oscillation cycle to prevent a build up, it is theorized that on the downstroke a gradual shedding occurs as the flow field adjusts to the decreasing angle of attack. In effect, the concept has successfully suppressed compressible dynamic stall over the basic airfoil through vorticity management.

Static pressure distributions over the airfoil with the Gurney flap showed that the lower surface pressures were slightly higher over all due to the stagnation of the stream against the flap. The flap also acts like an obstruction to the flow, causing separation from its lower edge. This separating shear layer meets the upper surface shear layer at a point downstream of the airfoil trailing edge and it is speculated that a vortex forms locally and effectively reduces the upper surface pressure there. The cumulative effect of these two factors leads to a higher total lift on the airfoil due to the use of the Gurney flap with the VDLE airfoil.

At M = 0.4, drooping the leading edge portion also eliminated the shocks that formed over the VR-12 airfoil, while giving results essentially similar to the that seen in Fig. 8b. This led to the conclusion that the VDLE concept is also effective when different stall onset mechanisms are involved.

3.4 Surface Vorticity Flux

As stated earlier, the surface vorticity flux distribution for each instantaneous angle of attack was calculated from the measured ensembled averaged pressure distributions and airfoil geometry. A cubic spline fit was used for deriving the pressure distributions at all the measured airfoil coordinates, from which the pressure gradients were obtained. The surface acceleration term in equation (1) was omitted for this calculation since it was determined to be about one order smaller. Fig. 9a presents the resulting distributions for the VR-12, the VDLE-VR-12 and the VDLE-VR-12 with 1% Gurney flap airfoils at two angles of attack, over the first 30% of the airfoil. Fig. 9b shows the same near the trailing edge region. The most striking result seen in Fig. 9a is that the peak surface vorticity flux is about 50% higher for the basic VR-12 airfoil compared to the other cases. As this is shed, a ‘wave” of vorticity flux travels down the airfoil for the basic airfoil and Fig. 9b shows that by α = 16 deg, this has reached x/c = 0.7. This wave represents the vorticity flux associated with the dynamic stall vortex as seen at the surface through its pressure imprint. The same trend was observed at lower Mach numbers, in some cases, the peak flux level at dynamic stall vortex formation for the basic airfoil was about 3 times that of the value derived for the VDLE cases. The vorticity flux downstream drops immediately once the vortex forms and starts convecting. However, near the leading edge, ahead of the suction peak a higher value of vorticity flux may still be seen for a few degrees after the vortex forms. This is because the boundary layer upstream of separation is still attached. The separation point moves upstream as the airfoil pitches-up and reaches the suction peak location at a slightly higher angle of attack. At that instant the local vorticity flux drops. Fig. 9 also shows that even though the two VDLE airfoils have slightly different geometries, the upper surface pressure gradients are almost identical. Since the airfoil geometry was modified such that the peak vorticity flux was reduced to prevent the dynamic stall vortex from forming, it can be said that vorticity management has brought about successful flow control.

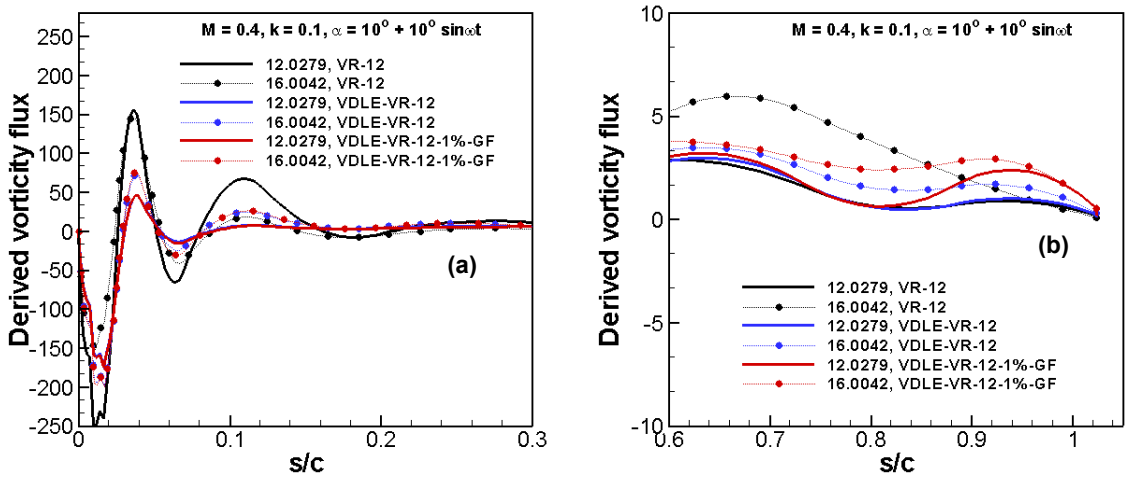

Fig. 9. Comparison of surface vorticity flux distributions over the different airfoil geometries; M = 0.3, k = 0.1, $\alpha = 10^{o}$-10^{o} sinωt; (a) Leading edge region (b) Trailing edge region

The picture near the trailing edge is somewhat different for all three cases. When the flow is attached, the vorticity is shed at a rate appropriate for that instantaneous flow condition, in effect maintaining a balance between the production and diffusion. Once the dynamic stall vortex passes the trailing edge, the level drops to zero for the VR-12 case. The VDLE airfoil has a small value since the vorticity is being shed from the shear layer enveloping the trailing edge flow separation, as the overall flow has not separated. The vorticity flux for the 1% Gurney flap shows an even higher value as seen by its rise before the trailing edge (the forced equality of the pressure at the trailing edge artificially causes all distributions to converge there). This seems to indicate that there is a small vortex trapped between the upper and lower surface shear layers (as suggested in Sec. 3.3). It also contributes to the total lift generated by the Gurney flapped airfoil.

3.5 Role of Transition

One of the least understood aspects of the dynamic stall problem is the role of transition. Due to the large angle of attack variation involved in a pitch-up maneuver, the transition point moves dramatically. This is even more critical for laboratory scale testing, where the Reynolds number could be in the transitional range. In this case, the dynamic stall onset mechanism can change rapidly as discussed in [1]. Fig. 10 shows the transition behavior for an NACA 0012 airfoil (for which a comprehensive set of data is in hand, [7]) at compressible speeds. It can be seen from Fig. 10a that the transition onset point moves from very near the trailing edge at $\alpha = 0$ deg to within a few percent of the leading edge at $\alpha \approx$ 6-8 deg. This large movement has not been modelled in any computational study of the flow. Increasing the freestream Mach number accelerates transition onset to occur at lower angles and further upstream, and increasing reduced frequency has an opposite effect, Fig. 10b. This movement generally occurs in the cases shown, *before* a laminar separation bubble or shocks form in the flow. Once either of these events occur, the dynamic stall onset mechanism is also affected by other following events, such as ability of the bubble to withstand the adverse pressure gradient and eventual bubble bursting or shock-interactions with the shear layer enveloping the bubble, instantaneous angle of attack, etc. Depending on where the boundary layer becomes turbulent, these factors influence the onset process differently. Furthermore, as the airfoil angle of attack is decreased on the

downstroke, a bubble can form again after the flow reattaches even partially, the flow relaminarizes at very low angles and these aspects have also not been modelled in any study. When a flow control method is implemented, these physical issues related to the boundary layer state could significantly alter its effectiveness. In the method reported here, drooping the airfoil leading edge largely neutralized compressibility effects over the leading 25% of the airfoil. This led to notable performance enhancements for all cases studied. However, since transition originates in the trailing portion of the airfoil, the changing geometry at the 0.25c point could be expected to introduce as yet unknown interactions and an even more complex behavior of the transition point movement than depicted in Fig. 10. It is not easy to eliminate the problem by simply tripping the airfoil in the laboratory scale studies, because tripping an airfoil at these scales introduce other issues [8] that are very difficult to resolve at a general level. No attempts were made to trip the airfoil on the present study. But it is recognized here that optimising the droop schedule i.e. the time history of the droop angle variation in relation to the angle of attack variation requires a more detailed study of the effects of transition also.

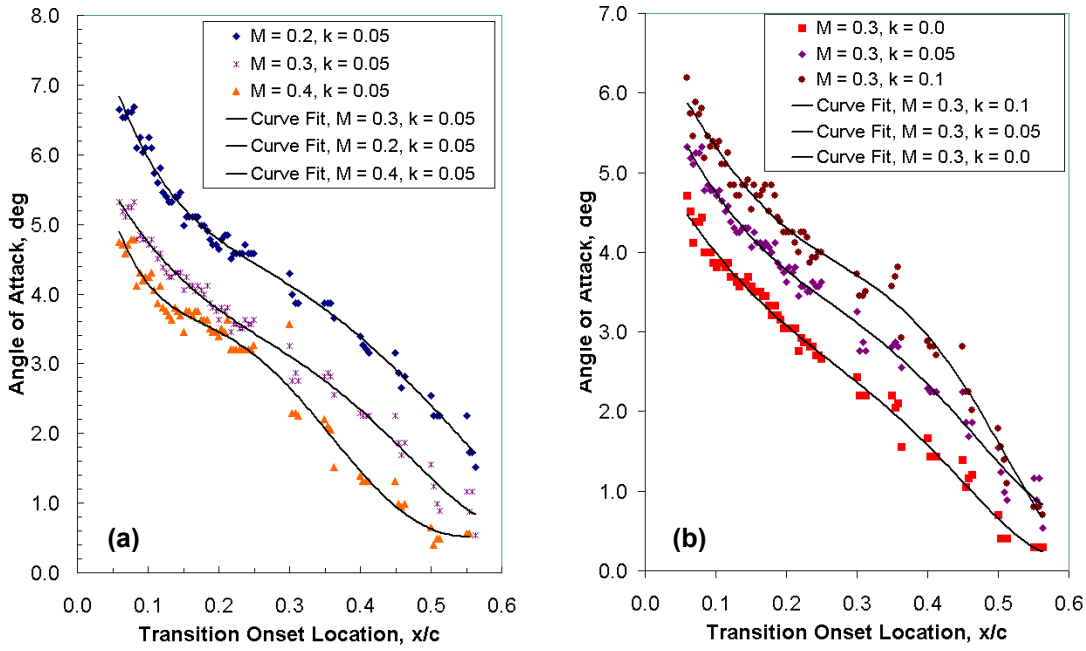

Fig. 10. Behavior of transition over an oscillating NACA 0012 airfoil, $\alpha=10^{O}+10^{O}\sin\omega t$; (a): Effect of Mach number, (b) Effect of reduced frequency [7]

3.6 General Discussion

This study has demonstrated successful compressible dynamic stall control through once per revolution actuation of the leading edge droop for specific cases of helicopter flight conditions. However, as Fig. 5 showed, a large hysteresis loop is present in the lift cycle. Ideally, the flow should reattach on the downstroke at much higher angles to reduce the hysteresis in order to retain the lift on the downstroke and to balance the loads on the advancing and retreating sides of a rotor blade. This requires complex tailoring of the droop schedule for each flow condition. A trial and error approach to determine these can prove to be unproductive

and expensive. It would be better to arrive at these through appropriate theoretical modelling of the problem. Since the flow changes presented were brought about from the effects of geometry changes on the potential flow, a simple potential modelling may seem of value here. However, the entire dynamic stall onset process is viscous in nature and is affected by the boundary layer behavior, some of which was discussed in the preceding section. Hence, any potential flow modelling would be inadequate and it is important to develop a fully viscous flow model that also incorporates the physics described in Sec. 3.5. When a droop schedule, as defined by the droop angle variation with angle of attack for each flow condition, is arrived at with such an approach, it may be possible to optimise the VDLE method with a more practical schedule for maximum L/D performance and minimum hysteresis of the lift cycle.

4. CONCLUSIONS

1. A novel compressible dynamic stall flow control method that droops the leading portion of an airfoil – the VDLE airfoil concept - synchronously with the sinusoidal pitch-up oscillations of the airfoil was successfully demonstrated.

2. Results showed that the undesirable consequences of a dynamic stall vortex were significantly reduced due to the vortex being virtually eliminated, giving as much as 75% reduction in drag and 50% decrease in the pitching moment coefficients, with only about 10% lift decrease.

3. Attaching a small (1%-chord high) Gurney flap to the trailing edge enabled recovering this loss of lift without an undue increase in drag.

4. Compressibility effects on dynamic stall were substantially reduced by the use of the VDLE concept, leading to the results described above.

5. Modification of the airfoil pressure distributions through which the peak vorticity flux was reduced to as little as a third of a basic airfoil was shown to be the reason for the observed effects.

6. Analytical studies that address the transition issues of the airfoil boundary layer would aid in the design of droop schedules that may help eliminate the large hysteresis seen in the lift behavior.

5. ACKNOWLEDGEMETS

This work was supported by the US Army Research Office, US Army Aeroflightdynamics Directorate (AFDD) and NASA through grants to the Naval Postgraduate School. Additional support instrumentation for instrumentation was received from AFDD. These sources of support are greatly appreciated.

6. REFERENCES

[1] M.S.Chandrasekhara, M.C.Wilder, and L.W.Carr, "On the Competing Mechanisms of Compressible Dynamic Stall," (AIAA Paper 96-1953), *AIAA Journal*, Vol. 36, No. 3, March 1998, pp. 387-393.

[2] L.W.Carr, M.S.Chandrasekhara, and N.Brock, "A Quantitative Study of Unsteady Compressible Flow on an Oscillating Airfoil," (AIAA Paper 91-1683), *Journal of Aircraft,* Vol. 31, No. 4, Jul.- Aug. 1994, pp. 892 - 898.

[3] W.C.Reynolds, and L.W. Carr, "Review of Unsteady, Driven, Separated Flows," AIAA Paper 85-0527, 1985.

[4] M.S. Chandrasekhara, P.B. Martin and C. Tung, "Compressible Dynamic Stall Control using a Variable Droop Leading Edge Airfoil," AIAA Paper No. 2003-0048, To appear in *Journal of Aircraft*.

[5] M.S. Chandrasekhara, P.B. Martin and C. Tung, "Compressible Dynamic Stall Performance of a Variable Droop Leading Edge Airfoil with a Gurney Flap," AIAA Paper No. 2004-0041, Jan. 2004.

[6] N.Brock, M.S.Chandrasekhara, and L.W.Carr, "A Real Time Interferometry System for Unsteady Flow Measurements," *ICIASF'91 RECORD*, IEEE Publication 91CH3028-8, pp. 423-431.

[7] M.S.Chandrasekhara, and M.C. Wilder, "Heat Flux Gage Studies of Compressible Dynamic Stall," (AIAA Paper 2002-0291) AIAA Journal, Vol.41, No. 5, May 2003, pp. 757-762.

[8] M.S.Chandrasekhara, M.C.Wilder, and L.W.Carr, "Boundary Layer Tripping Studies of Compressible Dynamic Stall Flow," (AIAA Paper 94-2340), AIAA Journal, Vol. 34, No. 1, Jan. 1996, pp. 96-103.

AVT-111 Specialists' Meeting on Enhancement of NATO Military Flight Vehicle Performance by Management of Interacting Boundary Layer Transition and Separation

DISCUSSION

1. REFERENCE No. OF THE PAPER: 2
2. DISCUSSOR´S NAME: Dr. Koerner
3. AUTHOR´S NAME: Chandrasekhara *et al.*

QUESTION:

1. Don't you think that 25% flap extension is a bit too large?
2. As to the Gurney-flap, it produces a high pitch-down moment for the advancing blade condition. How do you manage this?

AUTHOR´S REPLY:

Firstly it is not a flap, it is the l. e. regime of the airfoil itself.

1. Could be. It was convenient to use in this experiment. But, since the suction peak region is distributed over a larger length on the upper surface, a length of 10-15% for the drooping position does not seem unreasonable, especially when interferograms show shock induced dynamic stall onset at x = 0,08.
2. The Gurney flap needs to be retracted for the advancing rotor.

1. REFERENCE No. OF THE PAPER: 2
2. DISCUSSOR´S NAME: Malmuth
3. AUTHOR´S NAME: Chandrasekhara *et al.*

QUESTION:

Comment: This seems like a new fully unsteady transition.

AUTHOR´S REPLY:

Indeed it is. The large α change in the dynamic stall introduces a very large movement of the transition onset point – a fact crucial to proper modelling of the flow. Since transition movement is a function of flow condition (as documented for NACA 0012, AIAA J. May 2003) and drooping leading edge changes the leading-edge flow behaviour dramatically, the required data of flow physics remain unavailable. Definitely a worthwhile research effort.